ACS OMEGA

Open Access

http://pubs.acs.org/journal/acsodf

Article

Well-Separated Photoinduced Charge Carriers on Hydrogen Production Using NiS_2/TiO_2 Nanocomposites

Sivagowri Shanmugaratnam,* Punniamoorthy Ravirajan, Shivatharsiny Yohi,* and Dhayalan Velauthapillai*

Cite This: *ACS Omega* 2024, 9, 1627−1633

Read Online

ACCESS | Metrics & More | Article Recommendations | Supporting Information

ABSTRACT: Photocatalytic hydrogen production is a sustainable and greenhouse-gas-free method that requires an efficient and abundant photocatalyst, which minimizes energy consumption. Currently, interests in transition metal chalcogenide materials have been utilized in different applications due to their quantum confinement effect and low band gaps. In this study, different wt % of NiS_2-embedded TiO_2 nanocomposites were synthesized by a facile hydrothermal method and utilized for photocatalytic hydrogen production under extended solar irradiation. Among the materials studied, the highest amount (4.185 mmol g^{-1}) of hydrogen production was observed with 15 wt % of the NiS_2/TiO_2 nanocomposite. The highest photocatalytic activity may be due to the well separation of photoinduced charge carriers on the catalyst, which was confirmed by the electrochemical studies. Thus, we believe that these photocatalysts are promising candidates for future applications.

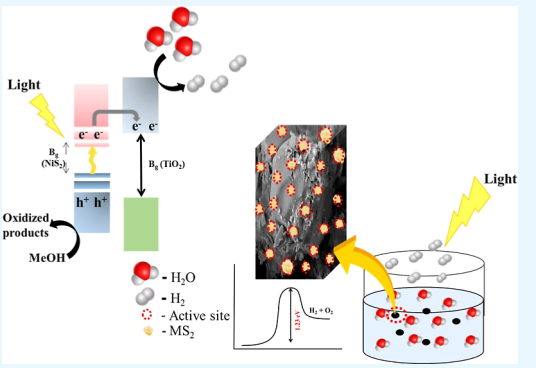

INTRODUCTION

The photon energy is harvested and converted into chemical fuels within the molecules of H_2 via a solar-driven water splitting process called photocatalytic water splitting.[1,2] Hydrogen produced by the photoreduction of water is an attractive reaction that will contribute to an ultimate green, sustainable chemistry and does not cause any unwanted emissions like carbon dioxide (CO_2) or carbon monoxide (CO), resulting in an energy revolution.[3,4] It is a multiple electron and multiple proton process. The sun shines on a catalyst which is dispersed in a pool of water, and then hydrogen gas is readily evolved; but the separation of the evolved H_2 from O_2 is disadvantageous for the photocatalytic process. The problem can be solved by using a Z-scheme photocatalyst system.

A direct Z-scheme photo catalyst possesses band structure configuration and distinctly different charge carrier transfer modes, as shown in Figure 1. In a Z-scheme charge carrier transfer pathway, the photogenerated electrons have strong reduction abilities in the conduction band (CB) of P1, while holes with strong oxidation abilities in the valence band (VB) of P2 are preserved. Simultaneously, the photo generated electrons in the CB of P2 and holes in the VB of P1, which have inferior redox power, tend to recombine.

Therefore, the Z-scheme photocatalyst possesses strong redox abilities for driving photocatalytic reactions and the spatially separated reductive and oxidative active sites. Furthermore, semiconductor photocatalysts with narrow band gaps can be chosen to construct direct Z-scheme

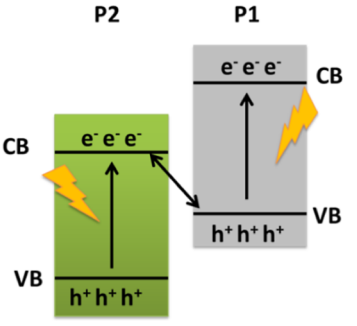

Figure 1. Z-Scheme electron transport.

photocatalysts, thereby broadening the light-harvesting range.[5] Moreover, this system has a catalyst in powder form and will be an added advantage for large-scale application of photocatalytic water splitting because of its simplicity.[6]

Since the first report on using a catalyst, TiO_2, for photoinduced water splitting in 1972 by Fujima Honda due to their significant characteristics that include strong optical absorption, favorable band edge position, abundant availability,

Received: October 18, 2023
Revised: November 30, 2023
Accepted: December 5, 2023
Published: December 19, 2023

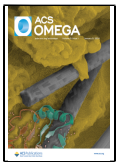

https://doi.org/10.1021/acsomega.3c08194
ACS Omega 2024, 9, 1627−1633

and nontoxicity,[1,6−8] a large number of semiconductor materials have been developed for different photocatalytic applications, such as metal oxides,[9,10] carbides,[11,12] metal chalcogenides,[13−18] graphene,[19−22] graphitic carbon nitrides,[23−28] and carbon nanotubes.[29−34] Among them, NiS_2 has attracted great attention because of its small band gap and high absorption coefficients, which make it suitable for photocatalytic activities by harvesting the visible light of the solar spectrum.[35] Therefore, it can overcome the limitations associated with photocatalysts that utilize UV irradiation.

Recently, Ma et al. utilized a facile method to synthesize two-dimensional NiS_2 on nickel foam (NF) for electrochemical hydrogen evolution. It was evidenced that the active sites of NiS_2 help to enhance the overall water splitting reactions.[36] In a separate study, NiS_2 catalysts were used to decorate the $CdLa_2S_4$ nanocrystals using the hydrothermal method for hydrogen generation under visible light irradiation. The NiS_2 loading enhances hydrogen production via the effective separation of electron hole pair. It was also noted in their study, the 2 wt % of NiS_2 loading exhibited remarkable enhancement in the production of hydrogen due to the activation effect of NiS_2 cocatalyst.[37] In addition to increasing the photocatalytic activity or efficiency, NiS_2 incorporated with titanium dioxide nanocrystalline develops Z-scheme nanocomposites.

Therefore, this study mainly focuses on synthesizing nanocomposites consisting of different weight percentages of NiS_2 embedded with titanium dioxide (TiO_2) using a facile hydrothermal method. These nanocomposites are intended to be used as photocatalysts for the production of hydrogen from water.

MATERIALS AND METHOD

Materials. Titanium isopropoxide, 98+% for the preparation TiO_2 was purchased from Sigma-Aldrich Norway AS, Oslo, Norway, $NiCl_2$ anhydrous (Sigma-Aldrich Norway AS) was employed as the precursor of NiS_2; and Na_2S (Sigma-Aldrich Norway AS), ACS reagent, as sulfur source and methanol (Analar NORMAPUR Reag. Ph.Eur., ACS).

Synthesis of NiS_2/TiO_2. $NiCl_2$ was taken in a beaker containing 40 mL of water. It was stirred with appropriate amount of TiO_2 (hydrothermal synthesis procedure used in previous studies[38] was followed here to synthesize this material) by sonication for 10 min at 50 °C. After that, the required amount of Na_2S was added in to it, and the mixture was stirred well. Then, the mixture was transferred into autoclave and kept at 140 °C for 10 h. The product was allowed to cool and centrifuged at 3000 rpm for 2 min and washed with ethanol followed by air drying. Pure NiS_2 nanomaterial was prepared by using a similar method without adding titanium dioxide.

Characterization. The above synthesized materials were characterized by using different techniques, such as powder X-ray diffraction (XRD) spectroscopy. The peak patterns were observed using D8 ADVANCE ECO in a 1 kW copper X-ray tube diffractometer with the scan range from 20 to 70° (2θ), The intensity of light reflected from the nanomaterials was measured using a diffuse reflectance spectroscopy (DRS Cary 100 Bio UV−visible spectrophotometer, Santa Clara, CA, USA) in the wavelength range of 800−200 nm. Scanning electron microscopy (SEM) was employed using Zeiss Supra 55 VP SEM, and the electro chemical measurements were performed with a Bio Logic SP-150 potentiostat.

Hydrogen Production. Hydrogen production experiment was carried out for the synthesized NiS_2/TiO_2 nanocomposite materials and the bare NiS_2 and TiO_2 materials. First, 20 mg of the catalyst was suspended in a 20 mL solution containing a 4:1(v/v) mixture of water−methanol mixture in which, methanol act as a hole-scavenger. The suspension was degassed for 60 min with nitrogen gas prior to irradiation. Then, suspensions were continuously stirred throughout the experiment. A 150 W xenon lamp (Oriel light source: Xenon arc lamp, Scientific Instruments) was used as the source of radiation. Finally, the amount of hydrogen gas produced during the reaction was measured using gas chromatography (Trace 1300, Thermo scientific) with a TCD (thermal conductivity detector). The same study was repeated with the pure water (without methanol) and pure methanol with and without catalysts for comparison purpose.

RESULTS AND DISCUSSION

The pure NiS_2, pure TiO_2, and different weight percentages of NiS_2 embedded titanium dioxide nanocomposite materials (5-, 10-, 15-, and 20-NiS_2/TiO_2) were successfully synthesized by the hydrothermal method, and the XRD results confirmed their formation (Figure 2). The figure further confirms the structural quality, purity, and phase orientations of the prepared nanocomposite materials.

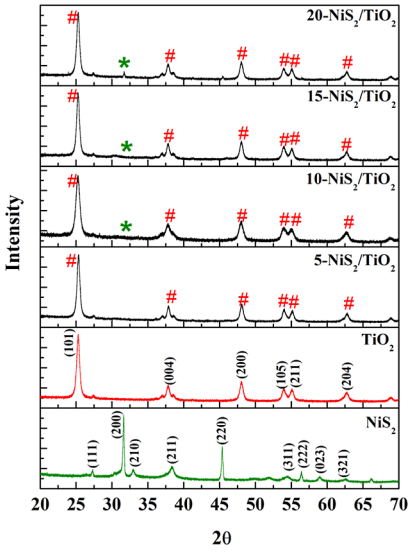

Figure 2. XRD patterns for pristine NiS_2, TiO_2, 5-, 10-, 15-, and 20-NiS_2/TiO_2 nanocomposites.

The Figure 2 confirms the formation of the anatase phase TiO_2 along with the crystal plane orientations evaluated by the diffraction angles 25.50, 37.76, 48.10, 53.88, 55.84, and 62.90° related to the planes of (101), (004), (200), (105), (211), and (204), respectively, authenticated from JCPDS 21-1272.[39] The peaks obtained at the 2θ values of 27.29, 31.63, 33.00, 38.30, 45.37, 54.49, 56.41, 59.02, and 62.52° due to (111), (200), (210), (211), (220), (311), (222), (023), and (321) diffraction planes of pure NiS_2 matched with JCPDS 11-0099.

The combined peak patterns observed with the mixed NiS_2/TiO_2 nanocomposite materials confirm the impregnation of NiS_2 on TiO_2 nanocrystalline. No other relevant peaks for oxides or any other compounds in XRD peaks further

https://doi.org/10.1021/acsomega.3c08194
ACS Omega 2024, 9, 1627−1633

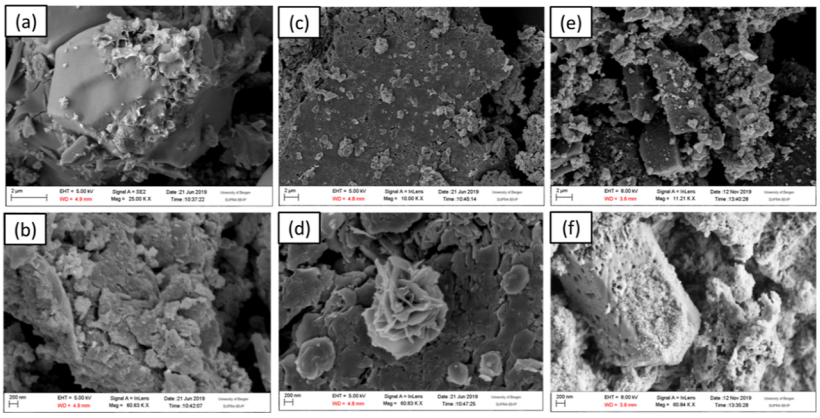

Figure 3. SEM images of NiS_2 (a,b), NiS_2/TiO_2 (c,d), and TiO_2 (e,f) nanomaterials.

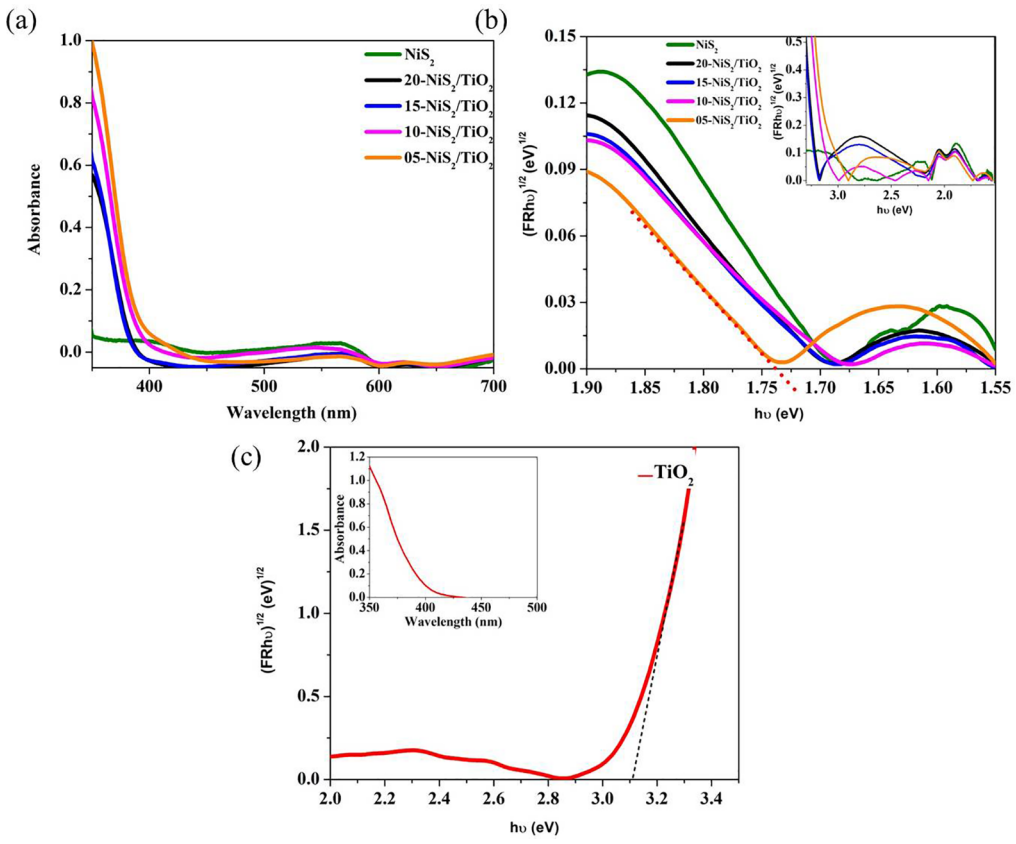

Figure 4. (a) Absorbance vs wavelength plot for NiS_2, 20-, 15-, 10-, and 5-NiS_2/TiO_2 materials, (b) Tauc plot for NiS_2, 5-, 10-, 15-, and 20-NiS_2/TiO_2 materials, and (c) Tauc plot for TiO_2 and onset shows absorbance vs wavelength plot.

confirmed that the NiS_2, TiO_2, and NiS_2/TiO_2 present in its pure forms.

Figure 3 shows the SEM images of pure NiS_2 (Figure 3a,b), 15 wt % of NiS_2 embedded TiO_2 nanocomposite (Figure 3c,d), and pure TiO_2 (Figure 3e,f). The SEM image of NiS_2 shows the flake-like structure material depicted in Figure 3a. The magnification image of Figure 3b clearly indicates the flake-like orientations of this material. Figure 3c,d shows the flake-like flower covered with spongy-like materials for NiS_2 embedded TiO_2 nanocomposites, which also further confirms the presence of NiS_2 on TiO_2 material. Pure TiO_2 materials exhibit a hexagonal rod-like material covered with spongy-like material illustrated in Figure 3e,f.

The weight ratio between Ni and Ti atoms were calculated by using energy-dispersive spectroscopy (EDS) and the values obtained were 4.03, 9.48, 13.82, and 20.11 for 5, 10, 15, and 20 wt % of NiS_2/TiO_2, respectively. The calculated values closely match the expected values; which are tabulated in Table S1.

The optical band gap of these photocatalytic materials, corresponding to the absorbance measurements obtained from DRS (Figure 4a), was determined by plotting the Tauc graph (Figure 4b), which was transformed via the Kubelka−Munk function. $\{[(R\infty)]$ vs E$\}$ when $n = 0.5$, for a direct allowed transition, $[K = (R\infty)]$ is an energy-independent constant. Estimates derived from the Tauc plots by extrapolating the steep portion of the plot in Figure 4b to the x-axis suggest the band gaps of these materials. The calculated band gap values of

https://doi.org/10.1021/acsomega.3c08194
ACS Omega 2024, 9, 1627−1633

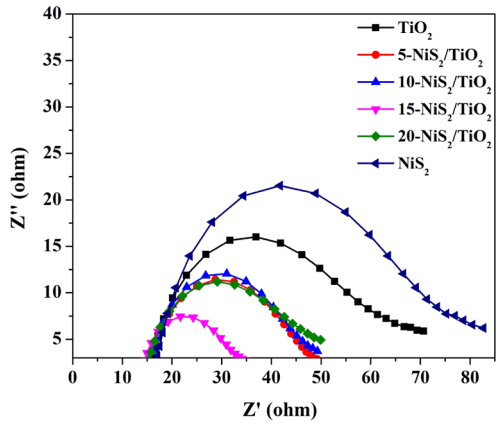

Figure 5. EIS Nyquist plots.

Table 1. R_s Values for TiO_2, NiS_2/TiO_2 (5, 10, 15, and 20) and NiS_2 Nanocomposites

materials	R_s value (Ω)
TiO_2	15.96
5-NiS_2/TiO_2	15.94
10-NiS_2/TiO_2	15.68
15-NiS_2/TiO_2	14.42
20-NiS_2/TiO_2	15.33
NiS_2	17.05

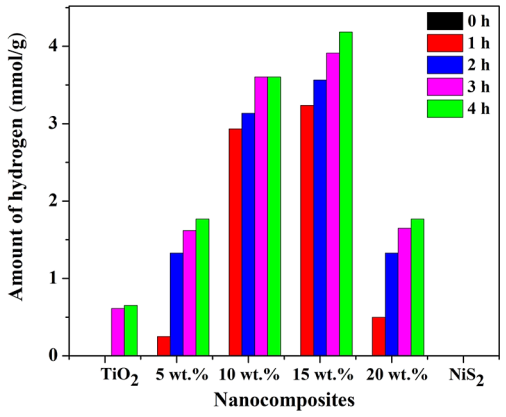

Figure 6. Amount of hydrogen evolution by using NiS_2, TiO_2, 5-, 10-, 15-, and 20-NiS_2/TiO_2 nanocomposites under extended solar irradiation.

nanocomposite materials are 1.738, 1.701, 1.699, and 1.695 eV for 5-, 10-, 15-, and 20-NiS_2/TiO_2, respectively. These values marginally decrease with increasing the amount of NiS_2 and are the intermediate values between pure NiS_2 (1.690 eV) and pure TiO_2 (3.100 eV).

Electrochemical impedance spectra (EIS), Nyquist plots of pristine TiO_2, NiS_2, and different wt % of NiS_2/TiO_2 (5-, 10-, 15-, and 20-NiS_2/TiO_2) nanocomposites are illustrated in Figure 5. The solution resistance values [(R_S = 14.42 Ω)] obtained from the EIS Nyquist plot of 15-NiS_2/TiO_2 is smaller than that of pristine TiO_2 (R_S = 15.96 Ω) and NiS_2 (R_S = 17.05 Ω) (Table 1). The arc radius of EIS spectra denotes the interface layer resistance occurring at the surface of the electrode. The smaller R_S value and arc radius indicate that there is a very low internal resistance and a higher interfacial charge transfer that improve separation of photoinduced charge carriers over the NiS_2/TiO_2 photocatalyst.[40,41]

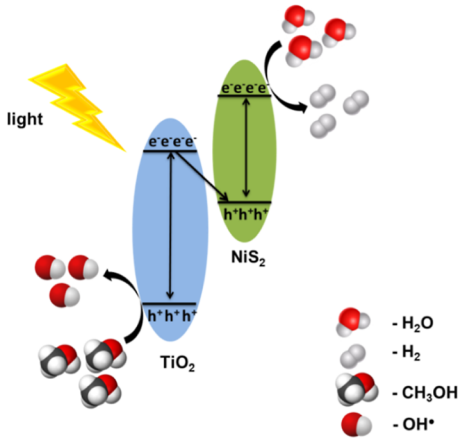

Figure 7. Schematic diagram for the Z-scheme photocatalyst.

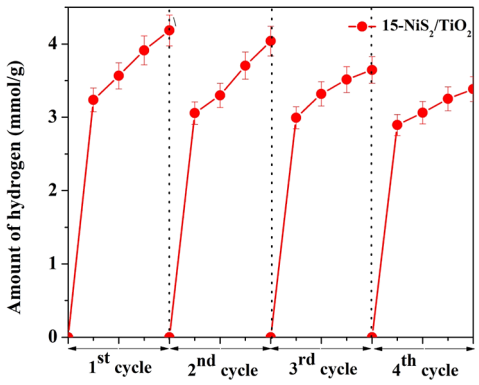

Figure 8. Amount of hydrogen production in four cycles by using 15-NiS_2/TiO_2 under extended solar irradiation.

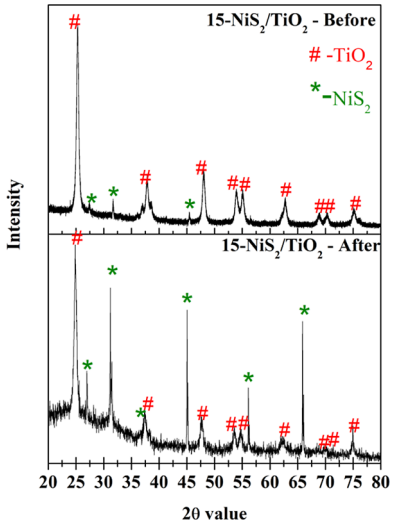

Figure 9. XRD pattern for 15 wt % of NiS_2/TiO_2 after four cycles of the hydrogen evolution reaction.

The amount of hydrogen evolution was measured with all catalysts prepared in this study under extended solar irradiation. The highest amount (4.185 mmol g^{-1}) of hydrogen evolution was attained with the 15-NiS_2/TiO_2 nanocomposite after 4 h of light illumination, whereas pure TiO_2 nanomaterial evolved only 0.651 mmol g^{-1}. Notably, no hydrogen was produced with pure NiS_2 material. An increasing trend in the

https://doi.org/10.1021/acsomega.3c08194
ACS Omega 2024, 9, 1627−1633

Table 2. Amount of Hydrogen Production with Different Chalcogenide Materials

material	synthesis method	light source	sacrificial agent	amount of hydrogen evolution[a]	reference
CuS	hydrothermal	450 W xenon lamp	NaS/Na_2SO_3	149 μmol g^{-1} h^{-1}	35
NiS_2				207 μmol g^{-1} h^{-1}	
FeS				636 μmol g^{-1} h^{-1}	
NiS_2 quantum dots on g-C_3N_4	hydrothermal	300 W xenon lamp equipped with a UV cut off filter (420 nm)	triethanolamine	4.8 μmol g^{-1} h^{-1}	43
RGO-NiS_2 synergistic modified g-C_3N_4 aerogel	thermal oxidation, etching-hydrothermal method	300 W xenon arc lamp	triethanolamine	1556 μmol g^{-1} h^{-1}	44
CdS/WS_2	impregnation-sulfidation	xenon lamp (300 W) (λ > 420 nm) to eliminate ultraviolet light	lactic acid	420 μmol h^{-1}	45
NiO Layer Over $Zn_{1-x}Cd_xS$	photodeposition	xenon lamp (HSX-UV 300) equipped with a 420 nm cutoff filter		99.9 μmol g^{-1} h^{-1}	46
dye-sensitized NiS_x on graphene	in situ chemical deposition	Hg lamp (400 W)	H_2PtCl_6	340 μmol h^{-1}	47
SnS_2/TiO_2	hydrothermal	150 W Xe arc lamp	methanol	196 μmol g^{-1}	16
CoS_2/TiO_2	hydrothermal	150 W Xe arc lamp	methanol	2550 μmol g^{-1}	38
NiS/TiO_2	solvothermal	300 W xenon lamp	lactic acid	698 μmol g^{-1} h^{-1}	48
NiS_2/TiO_2	**hydrothermal**	150 W **Xe arc lamp**	**methanol**	4185 μmol g^{-1}	**this study**

[a]Indicate unit variation and the lag in the literature to convert them into a particular unit.

hydrogen evolution was observed with the increase in the NiS_2 content on TiO_2 up to its 15 wt % and then it was found to decrease (1.766, 3.603, 4.185, and 1.767 mmol g^{-1} for 5, 10, 15, and 20 wt % NiS_2/TiO_2; Figure 6). The higher activity may be due to the well-separated electron hole pairs of the materials with smaller R_S value and arc radius indicate that there is a very low internal resistance and a higher interfacial charge transfer that improve separation of photoinduced charge carriers over the NiS_2/TiO_2 photocatalyst. Although similar band gap values were obtained with all the NiS_2/TiO_2 materials, impregnation of NiS_2 on TiO_2 that may lead the effective separation of electron−hole pairs due to the Z-scheme formation must be acknowledged for this higher H_2 production with 15-NiS_2/TiO_2.

In a typical mechanism, the photon hit on to the catalyst surface ejects the photon from the valence band to the conduction band, and the electrons move from the lower conduction band of TiO_2 to the higher valence of NiS_2 which neutralizes the holes and reduce the recombination with electrons.[42] On the other hand, methanol may oxidize when capturing the holes in TiO_2 as a sacrificial agent, which may inhibit the formation of oxygen gas (Figure 7). In addition, experimentally, no hydrogen was produced when pure water was tested with the catalyst and pure methanol was tested without the catalyst. Comparatively negligible amount of hydrogen (<0.012 mmol g^{-1}) was obtained with pure methanol with the catalyst under same experimental conditions.

The reusability and, thus, the stability of the catalyst were tested with the 15-NiS_2/TiO_2 material and are shown in Figure 8. Even after four cycles, the amount of hydrogen produced was found to be similar and there were no significant differences obtained (within 5% error) with the catalyst studied. These results indicate that the NiS_2/TiO_2 nanocomposite exhibited excellent stability in water. Furthermore, the structural characteristic was also tested with the used material (15-NiS_2/TiO_2) which was collected and dried after the experiment.

Figure 9 shows the XRD pattern of the 15 wt % of NiS_2/TiO_2 after its fourth cycle, and the peak patterns retained after the experiment indicate that the material is very stable. The XRD pattern shows an intense peak for NiS_2 compared to the initial material, which may be due to the amorphous nature of TiO_2 after the experiment.

Although a comparison of different studies is still questionable, it can be clearly seen that the catalyst prepared in this work exhibits a reasonably good amount of hydrogen and good stability. Comparing the results obtained in this study with the existing literature can indeed provide valuable insights into the performance of transition metal chalcogenide materials for hydrogen evolution. Despite the variations in experimental conditions, such as the light source, sacrificial agent, and synthesis method, which include carbon nitride, the comparison provides a clear picture of catalysts versus the amount of hydrogen produced. Different morphologies influence the amount of hydrogen production in many studies, as indicated in Table 2.

CONCLUSIONS

NiS_2/TiO_2 nanocomposite materials synthesized by the hydrothermal method exhibited a higher amount of (4.185 mmol g^{-1}) hydrogen evolution. The enhanced photocatalytic activity of the material (15-NiS_2/TiO_2) may be due to the effective electron−hole pair separation, which was supported by the electrochemical studies. Furthermore, the stability of the material can also add value to the use of these materials for future photocatalytic applications.

ASSOCIATED CONTENT

Supporting Information

The Supporting Information is available free of charge at https://pubs.acs.org/doi/10.1021/acsomega.3c08194.

Elemental dispersive spectra for 5-, 10-, 15-, and 20-NiS_2/TiO_2 nanocomposites and theoretical and experimental value of ratio between Ni and Ti from EDS analysis (PDF)

https://doi.org/10.1021/acsomega.3c08194
ACS Omega 2024, 9, 1627−1633

AUTHOR INFORMATION

Corresponding Authors

Sivagowri Shanmugaratnam − *Clean Energy Research Laboratory (CERL), Department of Physics, University of Jaffna, Jaffna 40000, Sri Lanka; Faculty of Engineering and Science, Western Norway University of Applied Sciences, Bergen 5020, Norway*; Email: sivagowrishanmugaratnam@gmail.com

Shivatharsiny Yohi − *Department of Chemistry, University of Jaffna, Jaffna 40000, Sri Lanka;* orcid.org/0000-0003-3920-1478; Email: srtharsha12@gmail.com

Dhayalan Velauthapillai − *Faculty of Engineering and Science, Western Norway University of Applied Sciences, Bergen 5020, Norway;* orcid.org/0000-0002-4162-7446; Email: Dhayalan.Velauthapillai@hvl.no

Author

Punniamoorthy Ravirajan − *Clean Energy Research Laboratory (CERL), Department of Physics, University of Jaffna, Jaffna 40000, Sri Lanka*

Complete contact information is available at: https://pubs.acs.org/10.1021/acsomega.3c08194

Author Contributions

Conceptualization, S.S. and Y.S.; methodology, S.S. and Y.S.; software, S.S.; validation, S.S., Y.S., D.V., and P.R.; formal analysis, S.S.; investigation, S.S. and Y.S.; resources, D.V., Y.S., and P.R.; data curation, S.S. and Y.S.; writing—original draft preparation, S.S.; writing—review and editing, S.S., Y.S., D.V., and P.R.; visualization, S.S and Y.S.; supervision, D.V., Y.S., and P.R.; project administration, D.V. and P.R.; and funding acquisition, D.V. and P.R. All authors have read and agreed to the published version of the manuscript.

Notes

The authors declare no competing financial interest.

ACKNOWLEDGMENTS

Higher Education and Research Collaboration on Nanomaterials for Clean Energy Technologies (HRNCET) project, grant number NORPART/2016/10237 and .RCN Project number: 333151 - FME HyValue - Norwegian center for hydrogen value chain research

REFERENCES

(1) Chen, J.; Wu, X. J.; Yin, L.; Li, B.; Hong, X.; Fan, Z.; Chen, B.; Xue, C.; Zhang, H. One-pot synthesis of CdS nanocrystals hybridized with single-layer transition-metal dichalcogenide nanosheets for efficient photocatalytic hydrogen evolution. *Angew. Chem., Int. Ed.* **2015**, *54*, 1210−1214.

(2) Nguyen, P. D.; Duong, T. M.; Tran, P. D. Current progress and challenges in engineering viable artificial leaf for solar water splitting. *J. Sci.: Adv. Mater. Devices* **2017**, *2*, 399−417.

(3) Martha, S.; Chandra Sahoo, P.; Parida, K. M. An overview on visible light responsive metal oxide based photocatalysts for hydrogen energy production. *RSC Adv.* **2015**, *5*, 61535−61553.

(4) Shanmugaratnam, S.; Yogenthiran, E.; Koodali, R.; Ravirajan, P.; Velauthapillai, D.; Shivatharsiny, Y. Recent Progress and Approaches on Transition Metal Chalcogenides for Hydrogen Production. **2021**, 1−37, doi: .

(5) Xu, Q.; Zhang, L.; Yu, J.; Wageh, S.; Al-Ghamdi, A. A.; Jaroniec, M. Direct Z-scheme photocatalysts: Principles, synthesis, and applications. *Mater. Today* **2018**, *21*, 1042−1063.

(6) Kudo, A.; Miseki, Y. Heterogeneous photocatalyst materials for water splitting. *Chem. Soc. Rev.* **2009**, *38*, 253−278.

(7) Jafari, T.; Moharreri, E.; Amin, A. S.; Miao, R.; Song, W.; Suib, S. L. Photocatalytic water splitting - The untamed dream: A review of recent advances. *Molecules* **2016**, *21*, 900−929.

(8) Rajaramanan, T.; Shanmugaratnam, S.; Gurunanthanan, V.; Yohi, S.; Velauthapillai, D.; Ravirajan, P.; Senthilnanthanan, M. Cost Effective Solvothermal Method to Synthesize Zn-Doped TiO_2 Nanomaterials for Photovoltaic and Photocatalytic Degradation Applications. *Catal. Artic.* **2021**, *11*, 690.

(9) Chakrabarti, S.; Dutta, B. K. Photocatalytic degradation of model textile dyes in wastewater using ZnO as semiconductor catalyst. *J. Hazard. Mater.* **2004**, *112*, 269−278.

(10) Liu, Y.; Xie, S.; Li, H.; Wang, X. A highly efficient sunlight driven ZnO nanosheet photocatalyst: Synergetic effect of p-doping and MoS2 atomic layer loading. *ChemCatChem* **2014**, *6*, 2522−2526.

(11) Vrubel, H.; Hu, X. Molybdenum Boride and Carbide Catalyze Hydrogen Evolution in both Acidic and Basic Solutions. *Angew. Chem., Int. Ed.* **2012**, *51*, 12703−12706.

(12) Chen, W. F.; Muckerman, J. T.; Fujita, E. Recent developments in transition metal carbides and nitrides as hydrogen evolution electrocatalysts. *Chem. Commun.* **2013**, *49*, 8896−8909.

(13) Yao, N.; Tan, T.; Yang, F.; Cheng, G.; Luo, W. Well-aligned metal-organic framework array-derived CoS2 nanosheets toward robust electrochemical water splitting. *Mater. Chem. Front.* **2018**, *2*, 1732−1738.

(14) Berkdemir, A.; Gutiérrez, H. R.; Botello-Méndez, A. R.; Perea-López, N.; Elías, A. L.; Chia, C. I.; Wang, B.; Crespi, V. H.; López-Urías, F.; Charlier, J. C.; et al. Identification of individual and few layers of WS_2 using Raman Spectroscopy. *Sci. Rep.* **2013**, *3*, 1−8.

(15) Mihai, C.; Sava, F.; Galca, A. C.; Velea, A. Low power non-volatile memory switching in monolayer-rich 2D WS_2 and MoS_2 devices. *AIP Adv.* **2020**, *10*..

(16) Shanmugaratnam, S.; Selvaratnam, B.; Baride, A.; Koodali, R.; Ravirajan, P.; Velauthapillai, D.; Shivatharsiny, Y. SnS_2/TiO_2 Nanocomposites for Hydrogen Production and Photodegradation under Extended Solar Irradiation. *Catalysts* **2021**, *11*, 589−612.

(17) Shanmugaratnam, S.; Rasalingam, S. Transition Metal Chalcogenide (TMC) Nanocomposites for Environmental Remediation Application over Extended Solar Irradiation. In *Nanocatalysts*, Sinha, I.; Shukla, M.; Eds. 2019, Chapter 6, page75

(18) Ning, X.; Lu, G. Photocorrosion inhibition of CdS-based catalysts for photocatalytic overall water splitting. *Nanoscale* **2020**, *12*, 1213−1223.

(19) Gautam, A. K.; Faraz, M.; Khare, N. Enhanced thermoelectric properties of MoS_2 with the incorporation of reduced graphene oxide (RGO). *J. Alloys Compd.* **2020**, *838*, 155673.

(20) Li, Y.; Wang, H.; Peng, S. Tunable photodeposition of MoS_2 onto a composite of reduced graphene oxide and CdS for synergic photocatalytic hydrogen generation. *J. Phys. Chem. C* **2014**, *118*, 19842−19848.

(21) Hintze, C.; Morita, K.; Riedel, R.; Ionescu, E.; Mera, G. Facile sol-gel synthesis of reduced graphene oxide/silica nanocomposites. *J. Eur. Ceram. Soc.* **2016**, *36*, 2923−2930.

(22) Chang, R. J.; Tan, H.; Wang, X.; Porter, B.; Chen, T.; Sheng, Y.; Zhou, Y.; Huang, H.; Bhaskaran, H.; Warner, J. H. High-Performance All 2D-Layered Tin Disulfide: Graphene Photodetecting Transistors with Thickness-Controlled Interface Dynamics. *ACS Appl. Mater. Interfaces* **2018**, *10*, 13002−13010.

(23) Li, Q.; Zhang, N.; Yang, Y.; Wang, G.; Ng, D. H. L. High efficiency photocatalysis for pollutant degradation with MoS_2/C_3N_4 heterostructures. *Langmuir* **2014**, *30*, 8965−8972.

(24) Liu, E.; Chen, J.; Ma, Y.; Feng, J.; Jia, J.; Fan, J.; Hu, X. Fabrication of 2D $SnS_2/g\text{-}C_3N_4$ heterojunction with enhanced H_2 evolution during photocatalytic water splitting. *J. Colloid Interface Sci.* **2018**, *524*, 313−324.

(25) He, K.; Xie, J.; Li, M.; Li, X. In situ one-pot fabrication of $g\text{-}C_3N_4$ nanosheets/NiS cocatalyst heterojunction with intimate interfaces for efficient visible light photocatalytic H_2 generation. *Appl. Surf. Sci.* **2018**, *430*, 208−217.

(26) Zhang, Z.; Huang, J.; Zhang, M.; Yuan, Q.; Dong, B. Ultrathin hexagonal SnS_2 nanosheets coupled with g-C_3N_4 nanosheets as 2D/2D heterojunction photocatalysts toward high photocatalytic activity. *Appl. Catal., B* **2015**, *163*, 298−305.
(27) Zhang, Z.; Kang, Y.; Yin, L. C.; Niu, P.; Zhen, C.; Chen, R.; Kang, X.; Wu, F.; Liu, G. Constructing CdSe QDs modified porous g-C_3N_4 heterostructures for visible light photocatalytic hydrogen production. *J. Mater. Sci. Technol.* **2021**, *95*, 167−171.
(28) Hong, J.; Wang, Y.; Wang, Y.; Zhang, W.; Xu, R. Noble-metal-free NiS/C_3N_4 for efficient photocatalytic hydrogen evolution from water. *ChemSusChem* **2013**, *6*, 2263−2268.
(29) Olowoyo, J. O.; Kumar, M.; Jain, S. L.; Babalola, J. O.; Vorontsov, A. V.; Kumar, U. Insights into Reinforced Photocatalytic Activity of the CNT - TiO_2 Nanocomposite for CO_2 Reduction and Water Splitting. *J. Phys. Chem. C* **2019**, *123*, 367−378.
(30) Moya, A.; Barawi, M.; Alemán, B.; Zeller, P.; Amati, M.; Monreal-bernal, A.; Gregoratti, L.; De, V. A.; Shea, P. O.; Vilatela, J. J. Interfacial studies in CNT fi bre/TiO_2 photoelectrodes for efficient H_2 production. *Appl. Catal., B* **2020**, *268*, 2−9.
(31) Hsieh, S.; Chen, W. Synthesis and Characterization of TiO_2/CNT Nanocomposites for Azo Dye Degradation. *Mater. Sci. Forum* **2017**, *909*, 243−248.
(32) Tahir, M. La-modified TiO_2 /carbon nanotubes assembly nanocomposite for efficient photocatalytic hydrogen evolution from glycerol-water mixture. *Int. J. Hydrogen Energy* **2019**, *44*, 3711−3725.
(33) Batmunkh, M.; Macdonald, T. J.; Shearer, C. J.; Bat-Erdene, M.; Wang, Y.; Biggs, M. J.; Parkin, I. P.; Nann, T.; Shapter, J. G. Carbon Nanotubes in TiO_2 Nanofiber Photoelectrodes for High-Performance Perovskite Solar Cells. *Adv. Sci.* **2017**, *4*, 1−11.
(34) Wang, J.; Wang, Z.; Zhu, Z. Synergetic effect of $Ni(OH)_2$ cocatalyst and CNT for high hydrogen generation on CdS quantum dot sensitized TiO_2 photocatalyst. *Applied Catal. B, Environ.* **2017**, *204*, 577−583.
(35) Huerta-Flores, A. M.; Torres-Martínez, L. M.; Moctezuma, E.; Singh, A. P.; Wickman, B. Green synthesis of earth-abundant metal sulfides (FeS_2, CuS, and NiS_2) and their use as visible-light active photocatalysts for H_2 generation and dye removal. *J. Mater. Sci. Mater. Electron.* **2018**, *29*, 11613−11626.
(36) Ma, Q.; Hu, C.; Liu, K.; Hung, S. F.; Ou, D.; Chen, H. M.; Fu, G.; Zheng, N. Identifying the electrocatalytic sites of nickel disulfide in alkaline hydrogen evolution reaction. *Nano Energy* **2017**, *41*, 148−153.
(37) Yuan, Y. P.; Cao, S. W.; Yin, L. S.; Xu, L.; Xue, C. NiS_2 Co-catalyst Decoration on $CdLa_2S_4$ Nanocrystals for Efficient Photocatalytic Hydrogen Generation under Visible Light Irradiation. *Int. J. Hydrogen Energy* **2013**, *38*, 7218−7223.
(38) Shanmugaratnam, S.; Velauthapillai, D.; Ravirajan, P.; Christy, A. A.; Shivatharsiny, Y. CoS_2/TiO_2 in nanocomposites for hydrogen production under UV irradiation. *Materials* **2019**, *12*, 3882.
(39) Xing, J.; Li, Y. H.; Jiang, H. B.; Wang, Y.; Yang, H. G. The size and valence state effect of Pt on photocatalytic H_2 evolution over platinized TiO_2 photocatalyst. *Int. J. Hydrogen Energy* **2014**, *39*, 1237−1242.
(40) Chang, C. J.; Wei, Y. H.; Huang, K. P. Photocatalytic hydrogen production by flower-like graphene supported ZnS composite photocatalysts. *Int. J. Hydrogen Energy* **2017**, *42*, 23578−23586.
(41) Yang, J.; Wang, X.; Zhao, X.; Dai, J.; Mo, S. Synthesis of uniform Bi_2WO_6-reduced graphene oxide nanocomposites with significantly enhanced photocatalytic reduction activity. *J. Phys. Chem. C* **2015**, *119*, 3068−3078.
(42) Zhao, J.; Shi, R.; Li, Z.; Zhou, C.; Zhang, T. How to make use of methanol in green catalytic hydrogen production? *Nano Sel.* **2020**, *1*, 12−29.
(43) Xue, F.; Liu, M.; Cheng, C.; Deng, J.; Shi, J. Localized NiS_2 Quantum Dots on g-C_3N_4 Nanosheets for Efficient Photocatalytic Hydrogen Production from Water. *ChemCatChem* **2018**, *10*, 5441−5448.
(44) Pan, J.; Wang, B.; Dong, Z.; Zhao, C.; Jiang, Z.; Song, C.; Wang, J.; Zheng, Y.; Li, C. The 2D RGO-NiS_2 dual co-catalyst synergistic modified g-C_3N_4 aerogel towards enhanced photocatalytic hydrogen production. *Int. J. Hydrogen Energy* **2019**, *44*, 19942−19952.
(45) Zong, X.; Han, J.; Ma, G.; Yan, H.; Wu, G.; Li, C. Photocatalytic H_2 evolution on CdS loaded with WS_2 as cocatalyst under visible light irradiation. *J. Phys. Chem. C* **2011**, *115*, 12202−12208.
(46) Ning, X.; Zhen, W.; Zhang, X.; Lu, G. Assembly of Ultra-Thin NiO Layer Over $Zn_{1-x}Cd_xS$ for Stable Visible-Light Photocatalytic Overall Water Splitting. *ChemSusChem* **2019**, *12*, 1410−1420.
(47) Kong, C.; Min, S.; Lu, G. Dye-sensitized NiS_x catalyst decorated on graphene for highly efficient reduction of water to hydrogen under visible light irradiation. *ACS Catal.* **2014**, *4*, 2763−2769.
(48) Zhang, L.; Tian, B.; Chen, F.; Zhang, J. Nickel sulfide as co-catalyst on nanostructured TiO_2 for photocatalytic hydrogen evolution. *Int. J. Hydrogen Energy* **2012**, *37*, 17060−17067.

https://doi.org/10.1021/acsomega.3c08194
ACS Omega 2024, 9, 1627−1633